2005 WJTA American Waterjet Conference
August 21-23 2005 ● Houston, Texas

Paper 5B-1

ANALYTICAL CHARACTERIZATION OF FLASH RUST FORMED ON CARBON STEEL AFTER UHP WATERJETTING

Moavin Islam, Wayne McGaulley
Corrpro Companies, Inc.
Washington, DC

Mike Evans
NAVSEA 05M1
Washington, DC

ABSTRACT

It is well established that when steel components are cleaned by high-pressure (HP) or ultra high pressure (UHP) waterjetting the surface begins to oxidize or 'flash rust' within a short period of time. Rusting per se is also observed after mechanical cleaning (abrasive blasting) of steel surfaces. However, it has been postulated that the rusting observed with the two cleaning methods are 'different' in nature. The present paper provides results of an in-depth investigation dealing with the composition, the thickness and other characteristics of the flash rust formed on steel surfaces after UHP waterjetting. Three levels of flash rusting; no flash rust (NFR), light flash rust (LFR), and moderate flash rust (MFR) were examined, using different surface analytical techniques. These included: (a) SEM examination to characterize the morphology of the oxide, (b) EDS analysis to determine elemental composition of the specimen surface, (c) XPS (or ESCA) analysis to obtain quantitative information about the composition and depth profile of the oxide layer, and (d) Raman Spectroscopy for characterizing the type of oxide. For comparison, an atmospherically corroded steel sample was also analyzed using the same techniques.

Based on XPS and Raman Spectroscopy data the composition of the oxide film on flash rusted samples is a complex mixture of different forms of stoichiometric and non-stoichiometric oxides of iron but mainly FeO, Fe_2O_3, Fe_3O_4, hydrated Fe_3O_4 and FeOOH. Based on the depth profile data, the approximate average oxide thickness was found to be 473 nm (0.5 μm) for the NFR specimen, 2398 nm (2.4 μm) for the LFR specimen, and 18209 nm (18.2 μm) for the MFR specimen. The oxide on the atmospherically corroded sample is of a similar composition but with different distribution and proportion.

INTRODUCTION

It is well established that when steel components are cleaned by high-pressure (HP) or ultra high pressure (UHP) waterjetting, the surface begins to oxidize or 'flash rust' within a short period of time. Rusting per se can also be observed after mechanical cleaning (abrasive blasting) of steel surfaces. However, it has been postulated that the rusting observed with the two cleaning methods are 'different' in nature (Ellor, 2003; Schmidt, 1997). Based on experimentation and practical experience, there is a common concern for painting over any such rust since it may lead to poor coating performance. A general consensus has developed that the critical issue appears to be residual surface salts (incorporated in the rust) and their subsequent deleterious effects (osmotic blistering and under-film corrosion) on organic coatings (Ellor, 2003). It has been suggested that waterjetting of previously corroded substrates removes detrimental salts more efficiently than any sort of mechanical cleaning and thus waterjetting should be a preferred surface preparation technology (Schmidt, 1997, Alblas and van Londen, 1997).

The color of the 'flash rust' obtained after waterjetting is typically orange, red, or brown of various shades depending on the color of the underlying steel, the nature of the surrounding environment, and the duration of exposure to the environment (McGaulley, et. al., 2003). Currently, there is no quantitative or semi-quantitative technique to characterize or categorize the level (or grade) of flash rust. However, descriptive and visual standards are available (SSPC/NACE, 2002) and are routinely used in the waterjetting industry.

It has been observed that when an array of steel panels is sequentially cleaned by waterjetting, those cleaned first always show the highest degree of 'flash rusting' while those cleaned last always have the lightest amount of flash rust (Ellor, 2003). Ostensibly this is directly proportional to the amount and time that the various panels had water come in contact with the cleaned surfaces (Ellor, 2003). Mist from the last panels to be cleaned came in contact with the first cleaned panels and thus contributed to their corrosion. Due to lack of research into the effects of flash rusting on coating performance, most paint specifications require reworking a flash-rusted surface to reveal bare steel. Additionally, most paint manufacturers will not accept liability if their products are applied over (some grades of) flash rusting (Schmidt, 1997; McGaulley, et. al., 2003).

Based on literature (Brubaker and Phipps, 1979) and also as discussed by Ellor (2003), the composition of the corrosion product layer formed on iron and steel surfaces whether in air or in solutions, is some form of oxide or hydrated oxide of iron: FeO, (α or γ) Fe_2O_3, Fe_3O_4, FeO(OH). The structure of the oxide is cubic in nature and it grows in an epitaxial manner with the underlying metal (Brubaker and Phipps, 1979). The thickness of the air-formed film at room temperature is 15-30 Å (Angstrom). Thicker films would be expected with longer exposure times to the environment. Hence, it may be assumed that the composition of 'flash rust' is most likely one or a combination of these compounds depending on the exact conditions under which it is formed.

There seems to be a paucity of data regarding the exact compositional analysis of flash rust formed subsequent to waterjetting. Morphological studies and elemental analysis have been conducted (Calabrese and Allen, 1978) on rust formed on mechanically cleaned steel using SEM

(scanning electron microscope), EDAX (Energy Dispersive Analysis by X-rays), and EMPA (Electron Microprobe Analysis). However, the Calabrese and Allen study does not provide any information on the exact composition or the thickness of the rust layer.

In view of the above discussion, an extensive literature search was conducted in order to identify suitable analytical methods, which could be used to determine the composition and the thickness of flash rust formed on steel surfaces after waterjetting. It was apparent that a sensitive surface analytical technique or techniques would be required. The following techniques were eventually chosen:

1. SEM for morphological/topographical information
2. EDS (Energy Dispersive spectroscopy) also known as EDAX for elemental information
3. XPS (X-ray Photon Spectroscopy) also known as ESCA (Electron Spectroscopy for Chemical Analysis) for compositional analysis as well as depth profiling.
4. Raman Spectroscopy for compositional analysis.

EXPERIMENTAL WORK

Flash rusted carbon steel samples from a recent UHP waterjetting operation were utilized in the experimental investigation and included the following types:

- No flash rust (NFR)
- Light flash rust (LFR)
- Moderate flash rust (MFR)

It may be mentioned that the flash rusted samples were preserved initially by storing in inhibited paper wraps in a desiccator and later by vacuum sealing to prevent further oxidation of the surface. In addition to the flash rusted samples, a rusted carbon steel coupon from an outdoor exposure (OE) site (marine environment, exposure period ~12 months) was also examined. Specimens measuring approximately 25 mm x 25 mm (1 inch x 1 inch) were obtained from the various coupons by shearing (see Figure 1). All samples were stored in airtight glass jars until the time of examination.

The following experimental work was undertaken on the flash rusted and OE samples:

1. SEM examination to characterize the morphology of the oxide
2. EDS analysis to determine elemental composition of the specimen surface.
3. XPS analysis and depth profiling to obtain quantitative information about the composition of the oxide layer.
4. Raman spectroscopy to obtain compositional information of the surface oxide

Prior to conducting the above procedures, low magnification optical microscopic examinations and photographic documentation (Optical Microscopy) of the different sample surfaces were also conducted.

RESULTS

Optical Microscopy

Low magnification optical micrographs of the different samples are shown in Figures 2 through 5. The difference in appearance between NFR, LFR, and MFR is very distinct. The oxide coverage is non-uniform and the percentage coverage increases progressively from NFR to MFR. The oxide layer on the OE sample appears to be compact and more crystalline in nature.

SEM Examination

SEM micrographs of the different specimen surfaces in Figures 6 through 9 show the morphological and topographical characteristics of the oxide layer. The SEM examination revealed that the surface of the NFR sample had minute amounts of oxides, which is not readily visible to the naked eye or even at low magnification. The oxide on the LFR and MFR samples is amorphous and nodular in structure. The oxide layer on the OE sample is thick, compact and crystalline.

EDS Analysis

EDS analyses were conducted along with SEM examination to identify the elements in the oxide layers of the different samples. Representative data are presented graphically in Figures 10 through 13. The predominant elements detected on all samples were Fe and O. Trace amounts of Al, S and Si were also detected. It is not possible to obtain quantitative compositional information from EDS analyses. However, qualitative or at best semi quantitative information can be derived from a careful comparison of the peak energy heights of the different elements. Thus considering the peak heights of Fe and O in Figure 10 (representing a NFR surface) indicates that there is very little Fe oxide present. Similarly the peak height of Fe and O in Figure 12 (MFR) and Figure 13 (OE sample) indicates the presence of Fe oxide, most likely in the form of Fe_2O_3 or Fe_3O_4. It is important to note that no Cl was detected even in the OE sample, which was under marine exposure. The absence of Cl in the OE sample is not readily explained and needs further careful investigation. It has been suggested that through the corrosion process, the chloride ions could have migrated to local corrosion pits and thus they are not generally distributed on the surface. Therefore, more extensive probing may have been required to locate chloride.

XPS Analysis and Depth Profiling

Depth profiling was achieved by sputtering with Ar (Argon) ions. The depth profile results for the three flash rust specimens and the OE specimen are given in Figure 14 and show changes in both O concentration and Fe concentration as a function of depth. In each case the Fe and O concentrations start from relatively close values (low for Fe, high for O), but the rate of change with depth is clearly different for each specimen. The NFR specimen reaches 90 at.% Fe relatively quickly, while the LFR changes less rapidly and only achieves 80 at% Fe in the depth profile range. The Fe concentration increased even more slowly for the MFR specimen, and remained relatively constant in the depth profile region for the OE specimen. Also noteworthy is

the fact that both the MFR and the OE specimens follow a linear behavior while rates of change in the Fe and O concentrations are clearly non-linear in the near-surface regions of the LFR and NFR specimens.

The depth profiling of the NFR specimen reached beyond most of the interfacial region to the base metal. The other flash rust specimens, having significantly thicker corrosion product films, required much greater sputtering times. In the sputtering time afforded to the OE specimen there was little change in the Fe to O ratio, proving that for that specimen the corrosion product layer was much thicker than any flash rust specimen.

Data modeling of selected XPS results for Fe and O collected throughout the depth profiling process allowed for more exact determination and quantification of the corrosion product components on each sample as a function of depth. Further details about the exact compositions of the different iron-oxygen compounds are available elsewhere (Islam, et. al., 2005)

Typical corrosion products expected to form on a carbon steel surface that has been wetted with fresh water in atmosphere can include the following: FeOOH, Fe_2O_3, Fe_3O_4, $Fe(OH)_2$, along with amorphous non- stoichiometric oxides on mature corrosion products. Incorporated water is common. For corrosion products formed on carbon steel in marine environments similar components are expected, although the corrosion mechanisms and the relative quantities may differ due to the presence of large quantities of chlorides, and possibly industrial pollutants depending on geographic location.

The NFR specimen had elemental Fe, Fe_3O_4, FeOOH, and incorporated water present near the surface, with waters of hydration attached to the oxide and oxy-hydroxide species. At greater depth Fe_2O_3 replaced the Fe_3O_4 and FeOOH species with attached water molecules and non-stoichiometric FeO. The concentration of elemental Fe increased with depth. The concentration of incorporated water decreased with depth, and was not seen at all at the greatest depth examined. Closer to the corrosion product/metal interfacial area Fe_3O_4 was again noted, along with the non-stoichiometric FeO.

The LFR specimen also had elemental Fe, Fe_3O_4, FeOOH, and incorporated water present near the surface (the elemental Fe starting at a greater depth than the NFR specimen), with waters of hydration again attached to the oxide and oxy-hydroxide species. At greater depth the oxide species present were Fe_3O_4 and Fe_2O_3 with attached waters. At even greater depth the Fe_3O_4 concentration began to decrease, Fe_2O_3 was no longer seen, and FeO was found. The concentration of elemental Fe increased with depth, but not as rapidly as the NFR specimen, indicating greater oxide layer thickness variations. The concentration of incorporated water stayed fairly constant at the depths examined.

The MFR specimen had hydrated Fe_3O_4 and Fe_2O_3, incorporated water present near the surface (starting at a depth similar to the LFR specimen), and very little elemental Fe. At greater depth the Fe_3O_4 concentration dropped by several percent. The Fe_2O_3 concentration dropped more dramatically in the shallow part of the layer, and then maintained a more constant value throughout the analysis depth. The concentration of elemental Fe increased with depth, but not as rapidly as the previous specimens, again indicating ever-increasing layer thickness throughout

the specimen series. Unlike the earlier specimens, no FeO was seen. The highest metallic Fe concentration observed at the deepest depth analyzed for chemistry was only at 46 at%, while FeO was observed on the LFR specimen only when metallic Fe was greater than 60 at%. Like the LFR specimen, the concentration of incorporated water stayed fairly constant at the depths examined.

One difference seen in the OE specimen as compared to the flash rust specimens was that no elemental Fe was seen at any depth in the analysis region. This was not unexpected since the corrosion product layer was clearly visibly thicker than any other specimen. The amount of incorporated water was higher throughout this specimen than in the flash rust specimens, especially in the near surface region, even after a much longer pump down time due to the higher vapor pressure of this specimen. Hydrated Fe_3O_4 and FeOOH were found in the near surface region. Fe_3O_4 was present at roughly constant concentration throughout the analysis depth, and in the greater depth regions the hydrated Fe_2O_3 oxide appeared to replace FeOOH. Like the MFR specimen, no FeO was seen in the OE sample inspection region.

The depth profile spectra modeling results discussed above may be used to estimate the corrosion product thicknesses for the flash rust specimens. An assumption that the average thickness can be approximated by the thickness at which elemental Fe achieves 50 at% has been employed here. It should be noted however, that this is a rough approximation due to the obviously large variations in layer thickness even over the surface of an individual specimen. This method is not viable for the OE specimen since a complete depth profile spectra could not be obtained. Based on the depth profile data, the approximate average thickness is 473 nm (0.5 μm) for the NFR specimen, 2398 nm (2.4 μm) for the LFR specimen, and 18209 nm (18.2 μm) for the MFR specimen.

Raman Spectroscopy

Raman spectroscopic analyses conducted on the surfaces are summarized by the spectra shown in Figure 15. OE spectra generally show a strong peak at wave number 380 cm^{-1}, and lesser peaks at 252, 528, and 645 cm^{-1}. This pattern is characteristic of lepidocrocite, an oxide of iron having the composition FeOOH. γ-FeOOH is a compound that is generally found on the outer surfaces of rust formed on steel exposed to most OE atmospheres. A complete description of the structure, occurrence, and properties of these and other iron oxides can be found in Cornell and Schwertmann (2003).

The absence of akaganite (β-FeOOH) on the OE sample is noteworthy because this compound forms in the presence of chlorides, and might be expected in a severe atmosphere. The fact that it is absent is in agreement with the overall lack of chloride based on other techniques discussed above.

In contrast to OE, spectra from both white and black areas of the NFR show a relatively weak peak (note the difference in scales) at a wave number of about 667 cm^{-1}. This pattern is characteristic of magnetite (Fe_3O_4) a compound that is commonly found in the inner layers of steel rust, often at the steel surface.

In the case of LFR and MFR, Raman spectra of the black and white background again show the presence of magnetite, although there is also evidence of a minor amount of lepidocrocite, particularly in the case of MFR. Finally, spectra of the orange deposits on LFR and MFR are characteristic of lepidocrocite.

The above results suggest that a freshly water-jetted rusted steel surface has a thin magnetite film that probably represents the remnants of an adherent inner portion of the initial rust layer. Another possibility is that the magnetite forms on the freshly exposed steel surface by reaction with the relatively hot jetting water.

The results further suggest that flash rusting proceeds by the accumulation of patches of lepidocrocite on the original magnetite surface. Although the origin of these patches is not certain, the possibilities include: (a) they are precipitated from iron-saturated water which exudes from pits on the steel surface after jetting, or (b) they represent reaction products formed during the subsequent jetting of adjacent material. The second possibility is consistent with two observations mentioned earlier, namely: (1) that flash rusting is heaviest on areas that are waterjetted first and least on areas waterjetted last, and (2) flash rust halts immediately upon the end of waterjetting.

SUMMARY AND CONCLUSIONS

1. Low magnification optical images show a distinct difference between the different grades of flash rust observed on carbon steel after ultra high pressure (UHP) waterjetting.
2. The nature of the surface film on flash rusted surfaces can be characterized by electron-optical techniques such as SEM, EDS, XPS (ESCA) and Raman spectroscopy.
3. Based on XPS analysis as well as Raman spectroscopy, the composition of the oxide film on flash rusted samples is a complex mixture of different forms of stoichiometric and non-stoichiometric oxides of iron but mainly FeO, Fe_2O_3, Fe_3O_4, hydrated Fe_3O_4 and FeOOH
4. Based on the depth profile spectra and data modeling, the approximate average oxide thickness is 473 nm (0.5 μm) for the NFR specimen, 2398 nm (2.4 μm) for the LFR specimen, and 18209 nm (18.2 μm) for the MFR specimen.

ACKNOWLEDGEMENTS

The authors would like to acknowledge the following:

1. Dr. Robert Bayles of Naval Research Laboratories (NRL), Washington, DC for SEM and EDS analyses.
2. Dr. Charles Anderson, Dr. Lorrie Krebs, and Ms. Lalitha Katipelli of Anderson Materials Evaluation, Inc. Columbia, MD for XPS analysis and optical microscopy.
3. Mr. Herbert Townsend of Townsend Corrosion Consultants, Inc., Center Valley, PA for the Raman Spectroscopy analysis.

REFERENCES

1. Alblas, B. P. and van Londen, A.M. "The Effect of Chloride Contamination on the Corrosion of Steel Surfaces: A Literature Review," PCE, pp 16-25, February 1997.
2. Brubaker, G. R. and Phipps, P. B. P., Eds., Corrosion Chemistry, American Chemical Society, Washington, DC, p 140, 1979
3. Calabrese, C. and Allen, J. R. "Surface Characterization of Atmospherically Corroded and Blast Cleaned Steel," Corrosion, vol. 34 (10), 1978.
4. Cornell, R. M. and Schwertmann, U., The Iron Oxides: Structure, Properties, Reactions, Occurrences and Uses, Wiley, Europe, 2003.
5. Ellor, J. "Analysis of Flash Rust – Characterization of Rust on Coating Performance," Point paper, Version 1.0, Corrpro Companies, Inc., March 2003.
6. Islam, M, McGaulley, and Evans, M., manuscript under preparation, 2005.
7. McGaulley, Shaw, W. B. and Berry, F. "Flash Rusting: Characterization and Effect of Coating Performance," JPCL, pp 76-86, May 2003.
8. Pemberton, J. E. and Guy, A. L. "Raman Spectroscopy," Metals Handbook, vol. 10, Materials Characterization, Ninth Addition, American Society for Metals, Metals Park, OH, pp. 126-138, 1986.
9. SSPC-VIS 4/NACE VIS 7 "Guide and Visual Reference Photographs for Steel Cleaned by Waterjetting," SSPC, Pittsburg, PA; NACE, Houston, TX, 2002
10. Schmidt, R. F. "Ultra High Pressure Comes of Age for Surface Preparation – It's Time to Get the Salts off the work," NACE Corrosion/97, Paper No. 594, 1997.

NOMENCLATURE

SEM:	Scanning Electron Microscope
EDAX:	Energy Dispersive Analysis by X-rays
EDS:	Energy Dispersive Spectroscopy
EMPA:	Electron Microprobe Analysis
ESCA:	Electron Spectroscopy for Chemical Analysis
XPS:	X-ray Photon Spectroscopy
NFR:	No Flash Rust
LFR:	Light Flash Rust
MFR:	Moderate Flash Rust
OE:	Outdoor Exposure
HP:	High Pressure
UHP:	Ultra High Pressure
at.%:	atomic per cent
nm:	nanometer (10^{-9} meter)
μm:	micron (10^{-6} meter)
Å:	Angstrom

(A) (B) (C) (D)

Figure 1. Photograph of Different Specimens (25 mm x 25 mm) Prior to Testing: (A) No Flash Rust (NFR); (B) Light Flash Rust (LFR); (C) Medium Flash Rust (MFR), and (D) Outdoor Exposure (OE)
Note: Sample (D) was exposed in a marine environment for ~12 months. Flash rusted samples are from a recent UHP waterjetting operation.

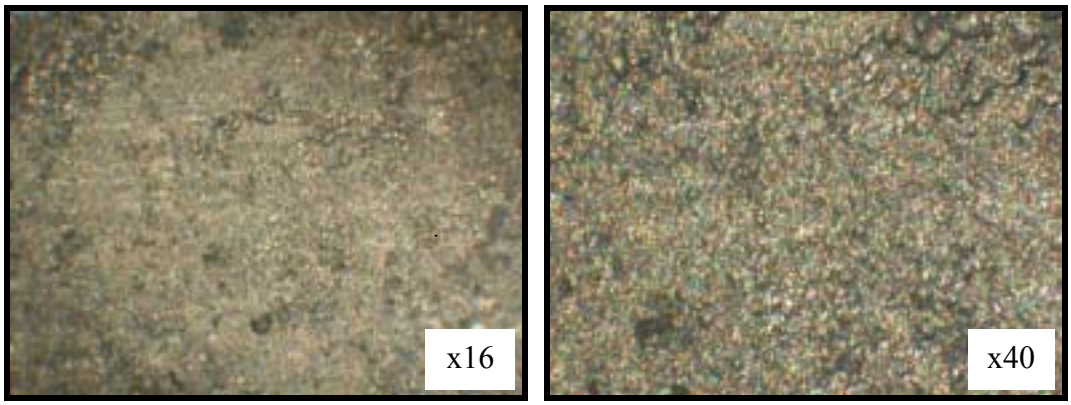

Figure 2. Optical Micrographs of No Flash Rust (NFR) Sample

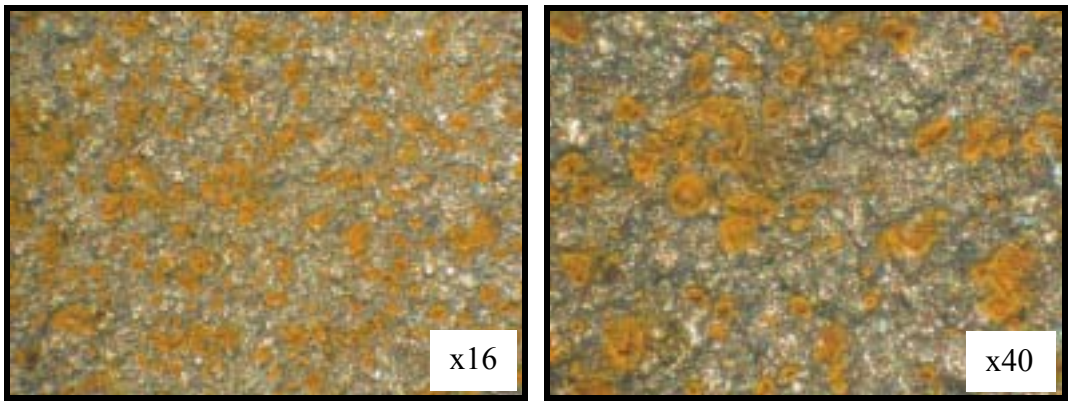

Figure 3. Optical Micrographs of Light Flash Rust (LFR) Sample

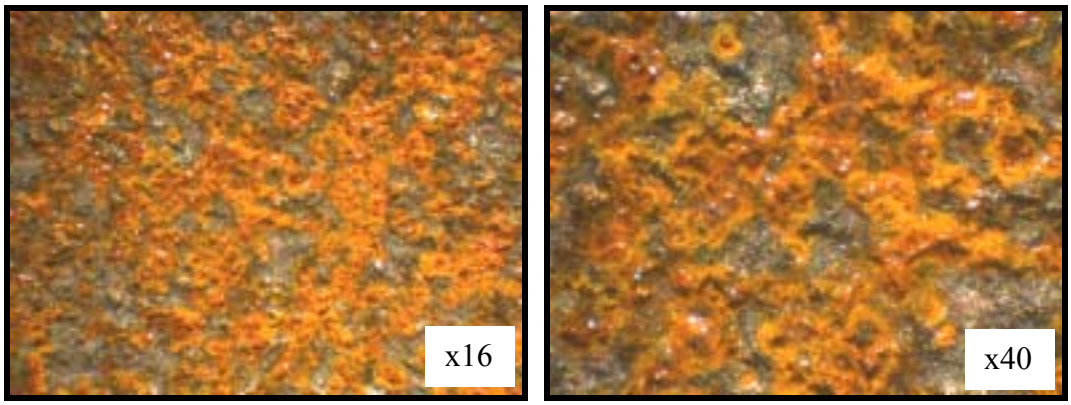

Figure 4. Optical Micrographs of Medium Flash Rust (MFR) Sample

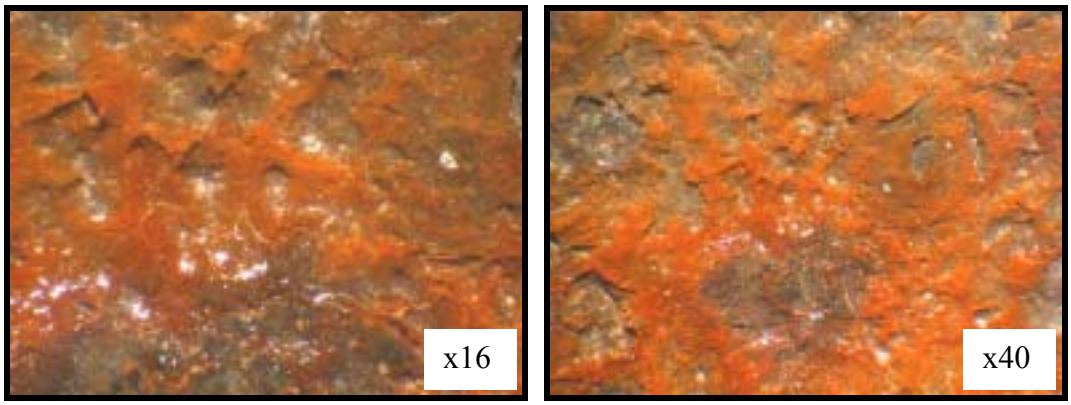

Figure 5. Optical Micrographs of Outdoor Exposure (OE) Sample

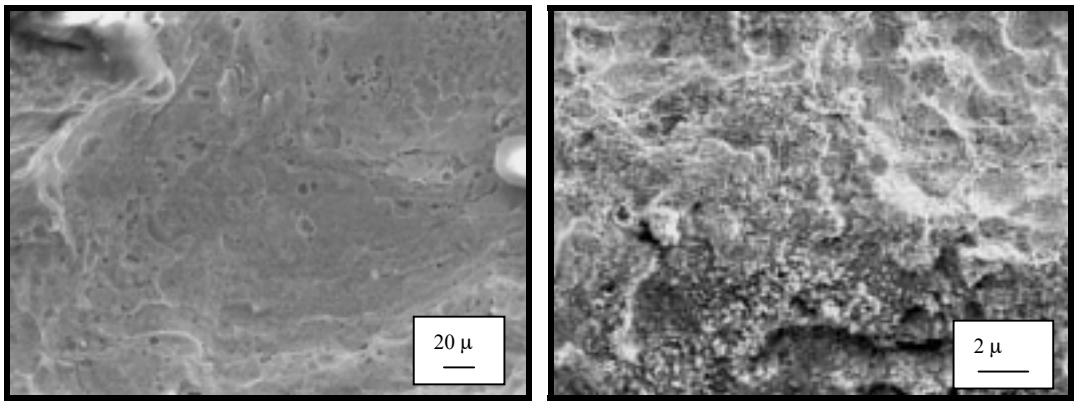

Figure 6. SEM Micrographs of No Flash Rust (NFR) Sample

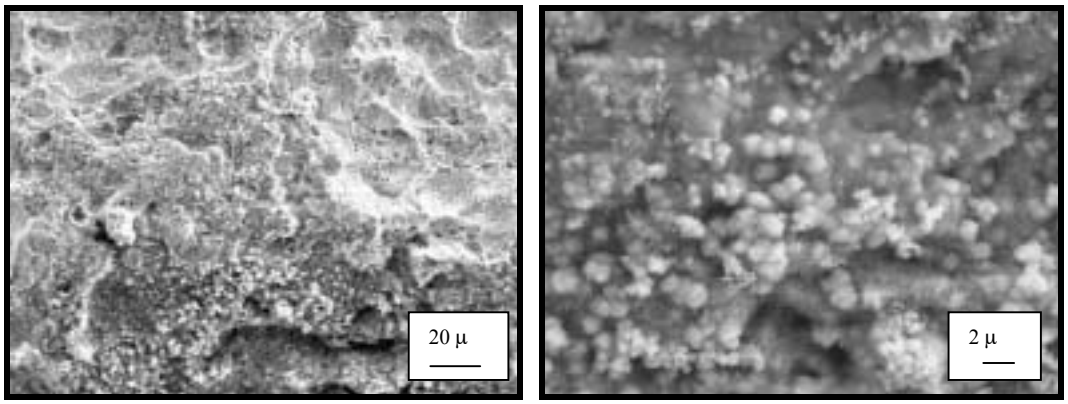

Figure 7. SEM Micrographs of Light Flash Rust (LFR) Sample

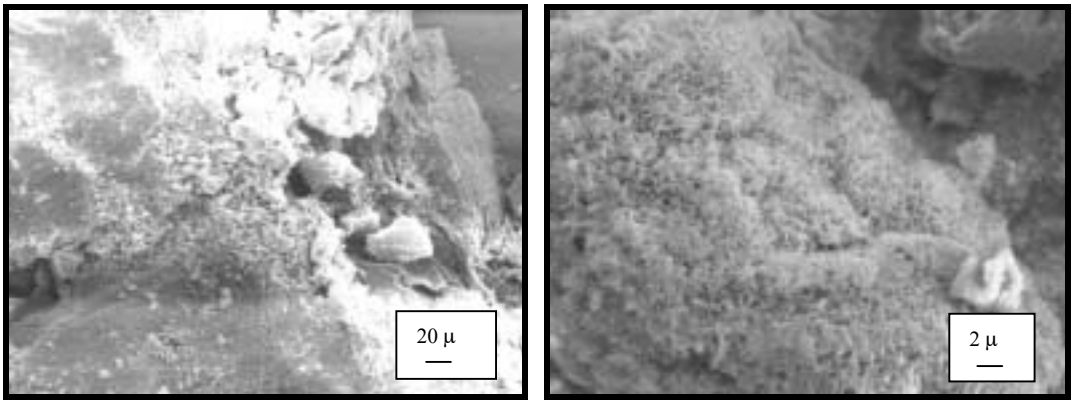

Figure 8. SEM Micrographs of Medium Flash Rust (MFR) Sample

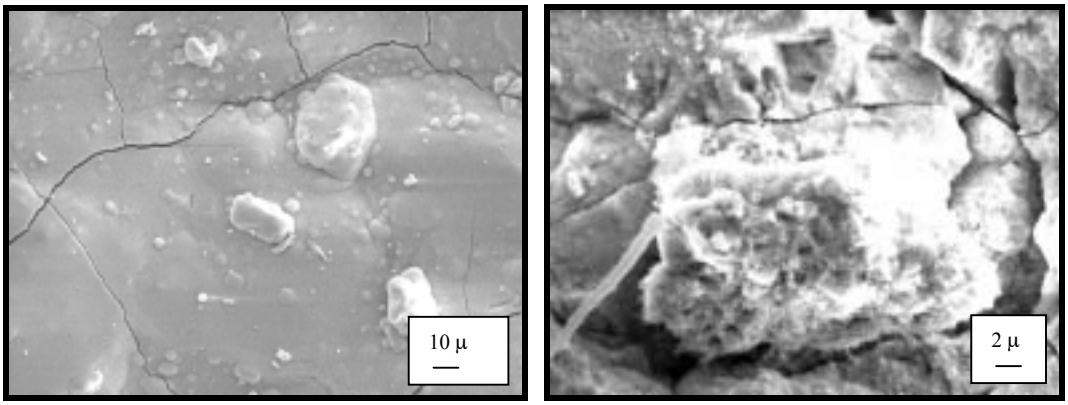

Figure 9. SEM Micrographsof Outdoor Exposure (OE) Sample

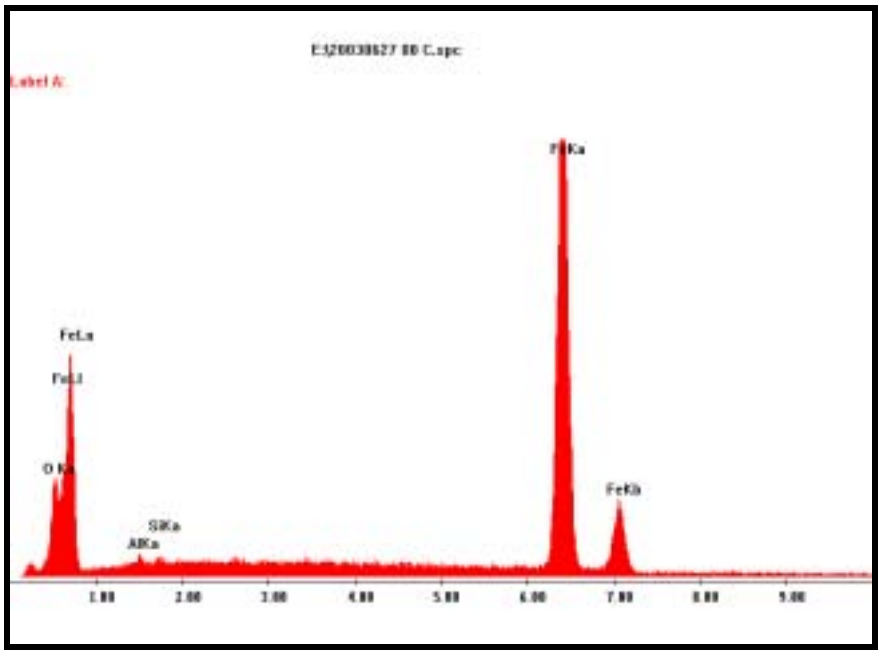

Figure 10. EDS Data for NFR Sample

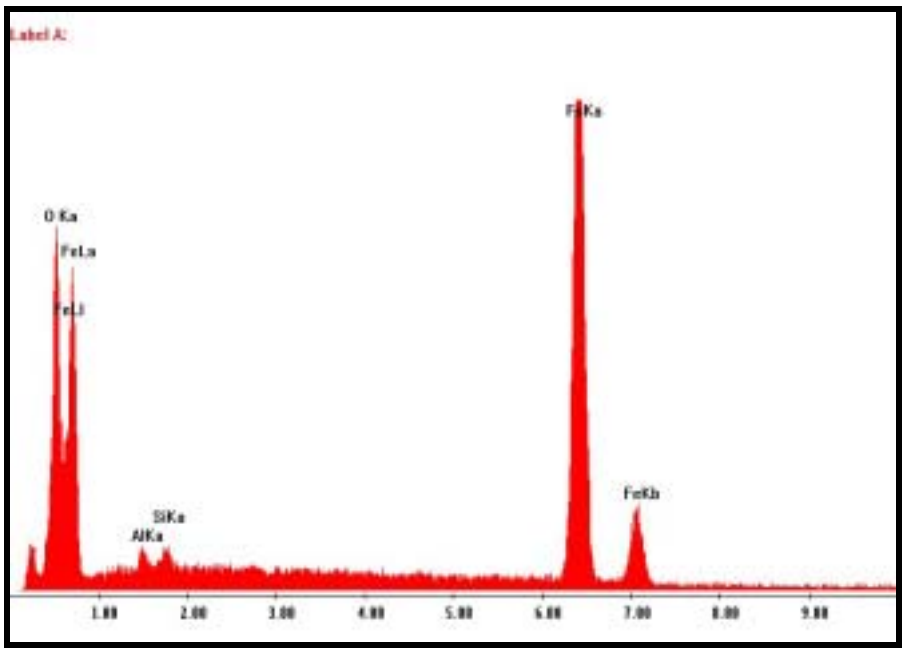

Figure 11. EDS Data for LFR Sample

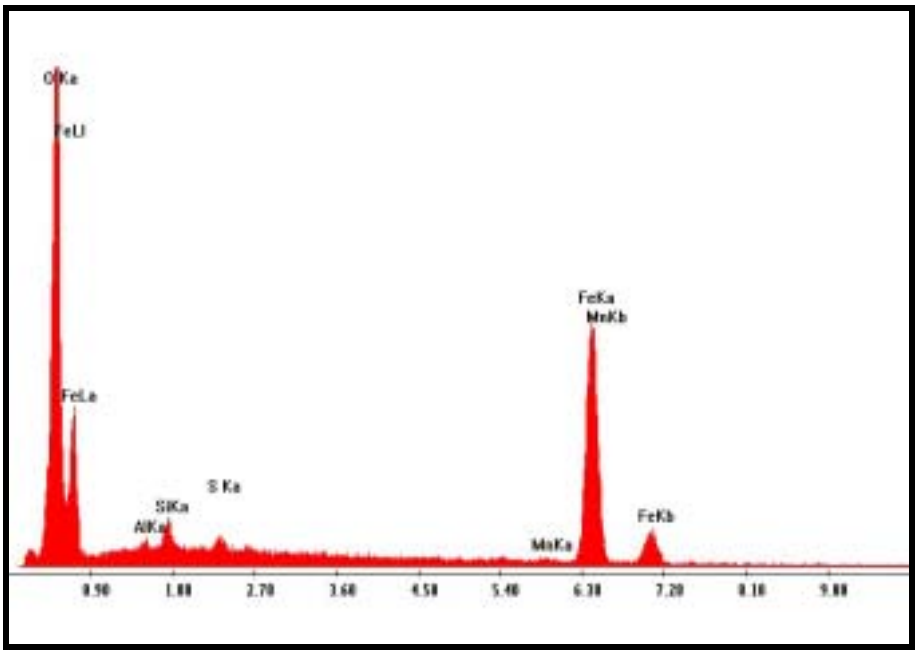

Figure 12. EDS Data for MFR Sample

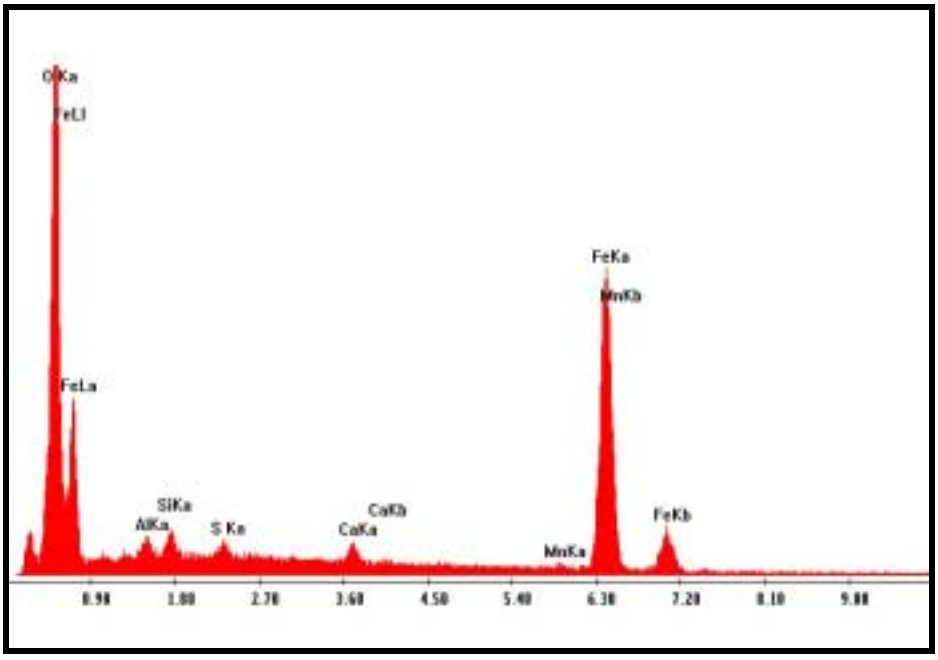

Figure 13. EDS Data for OE Sample

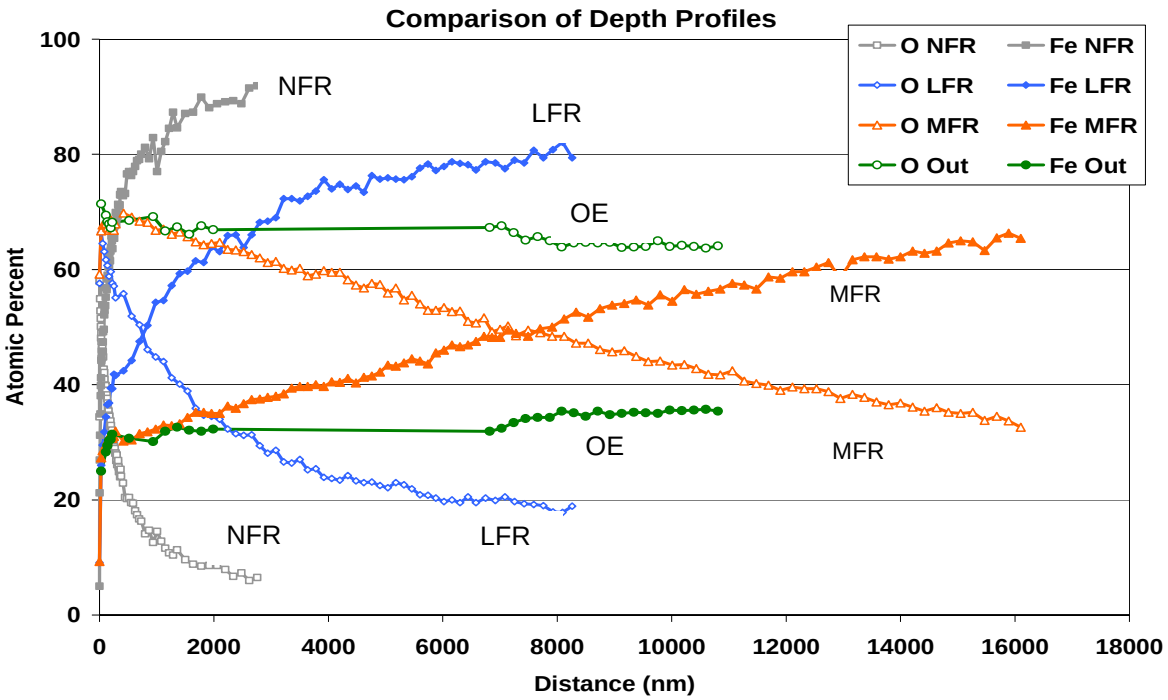

Figure 14. XPS Depth Profile Results for the Three Flash Rust Samples and One Outdoor Exposure Sample.
Open Symbols Indicate O (oxygen) Concentration as a Function of Depth
Closed Symbols Indicate Fe (iron) Concentration as a Function of Depth.

	Background	Rust deposits
No Flash Rust (NFR)	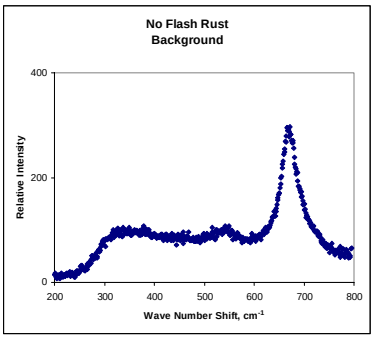	None
Light Flash Rust (LFR)	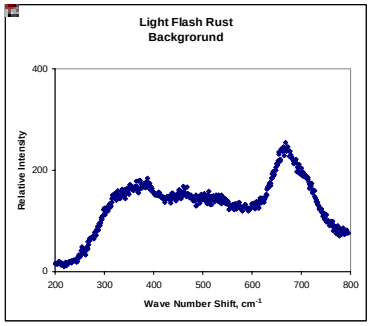	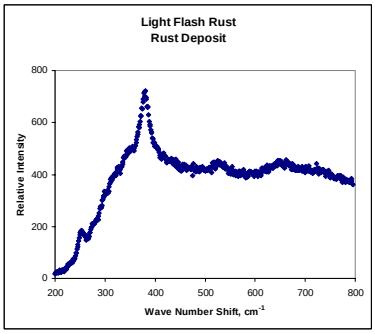
Moderate Flash Rust (MFR)	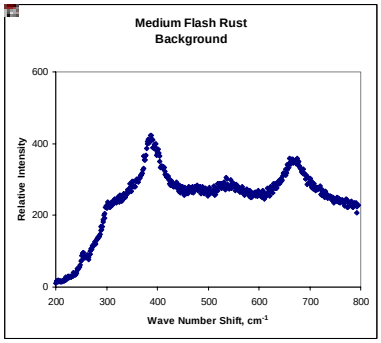	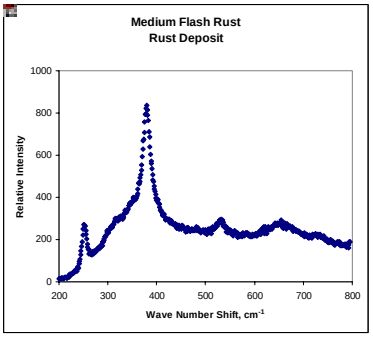
Outdoor Exposure (OE)	None	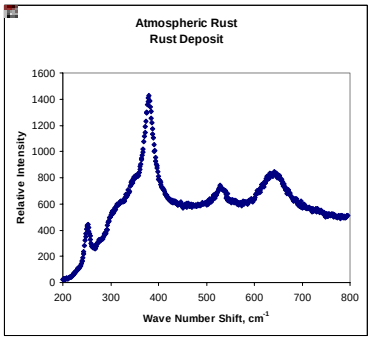

Figure 15. Typical Raman Spectra for Surfaces with Different Types of Rust